energies

MDPI

Article

Effect of the Dendrimer Generation Used in the Synthesis of Pt-Ru Nanoparticles Supported on Carbon Nanofibers on the Catalytic Activity towards Methanol Oxidation

Juan Carlos Calderón [1], Laura Calvillo [2], María Jesús Lázaro [2], José Luis Rodríguez [1] and Elena Pastor [1,*]

[1] Departamento de Química, Instituto de Materiales y Nanotecnología, Universidad de La Laguna, Avda. Astrofísico Francisco Sánchez s/n, 38206 San Cristóbal de La Laguna, Spain; jccalderong@yahoo.es (J.C.C.); jlrguez@ull.edu.es (J.L.R.)

[2] Instituto de Carboquímica—CSIC, Miguel Luesma Castán 4, 50018 Zaragoza, Spain; lauracalv@icb.csic.es (L.C.); mlazaro@icb.csic.es (M.J.L.)

* Correspondence: epastor@ull.edu.es; Tel.: +34-922-31-80-71

Academic Editor: Francesco Lufrano

Received: 30 November 2016; Accepted: 19 January 2017; Published: 28 January 2017

Abstract: Pt-Ru nanoparticles supported on carbon nanofibers (CNF) were synthesized by the sodium borohydride reduction method, using different generation dendrimers (zero, one, two and three generations). After the synthesis process, these materials were submitted to a heat treatment at 350 °C, in order to clean the nanoparticle surface of organic residues. TEM characterization showed that the Pt-Ru nanoparticles size ranged between 1.9 and 5.5 nm. The use of dendrimers did not totally avoid the formation of aggregates, although monodisperse sizes were observed. The heat treatment produces the desired surface cleaning, although promoted the formation of agglomerates and crystalline Ru oxides. The study of the electrochemical activity towards the methanol oxidation displayed some clues about the influence of both the dendrimer generation and the presence of Ru oxides. Moreover, the apparent activation energy E_{ap} for this reaction was determined. The results showed a beneficial effect of the heat treatment on the methanol oxidation current densities for the materials synthesized with the biggest dendrimers, being the methanol deprotonation and CO_{ad} diffusion the predominant rate determining steps (*rds*).

Keywords: Pt-Ru catalysts; carbon nanofibers; methanol electrochemical oxidation; dendrimers; fuel cells

1. Introduction

Many reports have described the interesting properties of dendrimers, related with their complexing properties [1–4] and hence, making them suitable molecules as encapsulating agents. They are macromolecules with a highly branched three-dimensional architecture, synthesized by means of an iterative sequence of reaction steps, each of them leading a higher generation molecule [4]. The branches define the dendrimer generation, being the first constituted by a monomer group linked to the molecule core. Subsequent union between monomers can be carried out, between other monomers and the end of the first monomer, constituting a second generation. Next generations are formed in the same way until steric hindrance avoids the attachment of other monomers [2]. Once dendrimers are assembled, they have free hollows for hosting metal precursors able to nucleate and form dendrimer encapsulated nanoparticles (DENs).

Some advantages associated to the use of dendrimers in the synthesis of nanoparticles are: (1) formation of nanoparticles with well-defined shape and size, due to the fairly uniform composition

and structure of dendrimers [5]; (2) stabilization of metal nanoparticles inside the dendrimer structure avoiding the formation of agglomerates [6]; (3) confinement through steric effects of encapsulated nanoparticles keep them unpassivated, enabling their participation in catalytic reactions [7]; (4) the dendrimer branches control the access of small substances to the catalytic nanoparticles [8]; (5) terminal groups on the dendrimer periphery can be modified to promote the solubility of the nanocomposite, facilitating the union with specific surfaces and polymers [8]. In general, the confinement of host species into the inner structure of the dendrimer is selective and depends on the host size, its nature, chemical composition and the inner surface of the cavity. Several interactions coordinate the host encapsulating, being some of them the formation of covalent bonds, electrostatic interactions, complex formation reactions, steric confinement, van der Waals forces and/or hydrogen bonds [4,9].

The synthesis of dendrimer-encapsulated nanoparticles (DENs) has taken high relevance, because of its potential for control nanoparticle size, composition [10] and dispersion on a surface [11]. Normally, this process consists of the complexation of metal precursors and then, a chemical reduction process using $NaBH_4$ or other reducing agent. The formation of nanoparticles in the dendrimer can be followed by the changes in solution color and the appearance of UV-visible absorbance bands [12], which are related with the final morphology [13,14]. Finally, metal nanoparticles can be supported on different materials [11,15–18] in order to be used in different applications.

Currently, the growth of nanoparticles into the dendrimer is an accepted fact if it possesses non-complexing functional groups on the periphery, such as hydroxyl groups [19,20]. The particle size depends on the numbers of metal ions complexed into the dendrimer [10,21–24], and also on the dendrimer cavity of the template in which the particles are prepared [25]. Nevertheless, when amine-terminated poly (amidoamine) dendrimers are employed as encapsulating agents, complexation can be realized on both the internal and peripheral amine groups [20,26], thereby promoting the formation of nanoparticles surrounded by surface amine groups from different dendrimers [27]. Protonation of the surface primary amine groups helps to prevent the metal complexation on the surface amine groups of dendrimers, restricting the formation of the particles to the internal part of the molecules and guaranteeing a more monodisperse particle size [28].

The synthesis of Pt-Ru nanoparticles has received great attention because of their feasibility to carry out the electrochemical oxidation of methanol when they are used as anodes in direct methanol fuel cells (DMFCs). Advantages of Pt-Ru alloys have been widely diseminated and these are related with the reduction of the production cost of DMFC anodes, performance increase and tolerance towards poisoning by CO, one of the intermediates generated during methanol oxidation [29–31]. Therefore, it is important to improve the synthesis methodologies for the preparation of these materials, with controlled metal content, atomic ratio and high electrochemical activity. Furthermore, the use of different reducing agents for metal precursors, such as sodium borohydride [29,32,33], formic acid [34–36], sodium formate [29,37], methanol [38] or polyols [39–41] has been reported. Different authors have reported the use of encapsulating agents as microemulsions [42,43] and dendrimers [44–46], in order to promote the control of nanoparticle size and their dispersion on the carbon support.

On the other hand, different carbon supports have been used in order to produce catalysts with better properties. Some of the most typical carbon supports are the carbon blacks [47–49], ordered mesoporous carbons [50–52] or carbon gels [43,46,53]. Particularly, carbon nanofibers promote the dispersion of Pt-Ru nanoparticles, enhancing the catalytic activity due to the carbon nanofiber-metal nanoparticle interactions and modifying the geometric characteristic of the crystallites [54]. Some factors such as the carbon nanofiber growth temperature are crucial for the activity of the catalysts; in fact, Sebastián et al. reported the effect of carbon nanofiber crystallinity and pore volumes of carbon nanofibers growth at different temperature on the activity of Pt-Ru supported catalysts [42].

In this work, we analyze the results obtained from the transmission electronic microscopy characterization of Pt-Ru nanoparticles supported on carbon nanofibers, which were synthesized making use of zero, one, two and three generation dendrimers. Particle sizes, polydispersion and

surface areas were correlated with both the generation of the employed dendrimer and the catalytic activity towards the methanol electrochemical oxidation, particularly, the apparent activation energy (E_{ap}) for this reaction. This parameter was calculated from stationary current densities at different applied potentials and temperatures [55], considering a treatment of the Arrhenius equation:

$$k = Ae^{-\frac{E_{act}}{RT}} \quad (1)$$

with k as the rate constant and A as a pre-exponential factor. k is proportional and inversely proportional to the developed current (i_a) and the electrode area (S), respectively [55]:

$$v = kC_R = \frac{i_a}{nFS} \quad (2)$$

so the current can be expressed as [55]:

$$i_a = A_{ap}e^{-\frac{E_{ap}}{RT}} \quad (3)$$

with A_{ap} and E_{ap} as the apparent pre-exponential factor and the apparent activation energy, respectively. By applying the logarithm function to the Equation (3), the apparent activation energy can be calculated from the lni_a vs. $1/T$ plot [55–59]:

$$lni_a = lnA_{ap} - \frac{E_{ap}}{RT} \quad (4)$$

considering that the slope of this plot is $m = E_{ap}/R$. In this way, knowing the slope values from the plots and the value for R (8.314 J·mol^{-1}·K^{-1}), it is possible to determine the values for E_{ap}.

2. Results and Discussion

2.1. Morphology and Physical Properties of the Synthesized Pt-Ru/CNF Catalysts

The studied catalysts were synthesized and physically characterized previouslty [45]. Table 1 reports the results obtained for the composition, particle/crystallite sizes, metal surface and electrochemical surface areas for the synthesized catalysts, which were determined in [45] and repeated in this work considering their importance to understand the electrochemical activity of the catalysts. The XRD patterns exhibited the typical face-centered cubic structure of platinum located at 40°, 47°, 68° and 82°, corresponding to the (111), (200), (220) and (311) crystalline reflections. Besides, an additional peak was observed toward 28.5°, especially in the case of the heat treated catalysts, which was assigned to the presence of Ru oxides formed after this treatment [45]. For the calculation of the crystallite size, the dimensions of the peak (220) of platinum has been used, bearing in mind there is no influence of the other crystalline plane reflections on this peak, allowing the establishment of a clear and accurate baseline. Then, the width of the peak in the middle-height and the peak value for this reflection are inserted in the Debye-Scherrer equation [60–62]:

$$d = \frac{0.9\ \lambda_{K\alpha 1}}{B_{2\theta}\cos\theta_{max}} \quad (5)$$

where $\lambda_{K\alpha 1}$ is the wavelenght of the employed X-ray radiation, $B_{2\theta}$ is the width of the peak in the middle-height, and θ is the maximun angle of the diffraction line. EDX analysis indicates that all catalysts had similar metal content and Pt:Ru atomic ratio, being comparable to those observed for the commercial Pt-Ru/C catalyst from E-TEK. These values were close to the nominal ones planned during the synthesis procedure, which corresponds to 20 wt. % for the metal content and 1:1 for Pt:Ru atomic ratio. This fact suggests that the synthesis method allows one to control the metal content and the atomic ratio, similar to the commercial catalyst nominal values and those synthesized by the same authors in the absence of any encapsulating agent in a previously reported work [29].

It must be highlighted that crystallite size values, which were calculated from the XRD patterns, resulted to be between 2.9 and 4.1 nm, being Pt-Ru/CNF-DN-3 TT the catalyst that exhibited the smallest size (2.9 nm) and Pt-Ru/CNF-DN-0 TT the largest one (4.1 nm). This effect was previously attributed to the low encapsulating capacity of the zero generation dendrimer, in contrast to the three-generation one [45]. Nevertheless, it must be taken into account that these values were calculated from the Pt (220) reflection, which is affected by the Ru oxides contribution, a fact observed in the catalysts DN-2, DN-1 TT, DN-2 TT and DN-3 TT (see Figure 2 in [45]). The metal surface areas were determined by means of the equation SA ($m^2 \cdot g^{-1}$) = 6 × 103/ρd [63], where d is the average crystallite size (nm) and ρ is the alloy density. To calculate ρ, it was considered that $\rho_{Pt\text{-}Ru}$ ($g \cdot cm^{-3}$) = $\rho_{Pt}X_{Pt} + \rho_{Ru}X_{Ru}$, with ρ_{Pt} = 21.4 $g \cdot cm^{-3}$ and ρ_{Ru} = 12.3 $g \cdot cm^{-3}$, and X_{Pt} and X_{Ru} as the weight percentage of Pt and Ru, respectively. The Pt-Ru/CNF-DN-0, Pt-Ru/CNF-DN-2, Pt-Ru/CNF-DN-3 and Pt-Ru/CNF-DN-3 TT catalysts displayed the highest metal surface areas, as a consequence of their low crystallite size. These results suggest that the high number of branches, especially present in the dendrimers DN-2 and DN-3 decrease the crystallite sizes and increase the metal surface areas, due to a favored dispersion of the nanoparticles on the carbon nanofibers.

Table 1. Composition, particle/crystallite sizes, metal surface areas (SA) and electrochemical surface areas (ECSA) of the synthesized PtRu catalysts.

Catalyst	Metal Loading (wt. %)	Atomic Ratio Pt:Ru	Particle Size/nm XRD	Particle Size/nm TEM	Metal Surface Area/$m^2 \cdot g^{-1}$	ECSA/$m^2 \cdot g^{-1}_{Metal}$
Pt-Ru/CNF-DN-0	12	58:42	3.3	3.7 ± 1.0	103	28
Pt-Ru/CNF-DN-0 TT	18	49:51	4.1	4.1 ± 1.4	87	21
Pt-Ru/CNF-DN-1	20	59:41	3.8	2.2 ± 0.5	89	32
Pt-Ru/CNF-DN-1 TT	17	52:48	3.6 [a]	1.9 ± 0.6	98	19
Pt-Ru/CNF-DN-2	20	44:56	3.0 [a]	2.0 ± 0.5	123	13
Pt-Ru/CNF-DN-2 TT	19	40:60	3.8 [a]	5.5 ± 1.5	99	28
Pt-Ru/CNF-DN-3	19	47:53	3.0	1.9 ± 0.4	121	7
Pt-Ru/CNF-DN-3 TT	21	41:59	2.9 [a]	3.1 ± 0.9	129	41
Pt-Ru/C E-TEK	20	45:55	4.4	4.5 [b]	76	42

[a] This data was calculated from the Pt (220) reflection, although a meaning error associated to the Ru oxides peaks overlaying on this peak is considered [45]; [b] This data is reported in [64].

In order to further investigate the effect of the dendrimer generation, TEM analysis was made in the present paper, with the purpose of determining the particle dispersion and a more accurate value for the particle sizes based in the size distributions. Figure 1 displays the TEM images for the catalysts synthesized with the four dendrimers (from zero to three). In the Pt-Ru/CNF-DN-0 catalyst, the formation of agglomerates with raceme-like shape is observed, resulting in a low dispersion of the nanoparticles on the carbon nanofibers. This is explained from the low size and molecular weight of the zero-generation dendrimer structure, having a lower number of branches, and therefore, a lower encapsulating capacity that results in the formation of bigger nanoparticles and agglomerates. Moreover, an improvement of the dispersion, as well as a decrease of the particle size (from 3.7 ± 1.0 nm for Pt-Ru/CNF-DN-0 to 1.9 ± 0.4 nm for Pt-Ru/CNF-DN-3), is achieved when the dendrimer generation increases (see Figure 2).

It should be considered that the increase of the dendrimer generation means an increase of the surface amino groups number per dendrimer molecule, being 4, 8, 16 and 32 for the 0, 1, 2 and 3 generations, respectively. In the synthesis, the number of Pt ions for each dendrimer molecule was set to 55 in all cases. Then, the theoretical size value for a 55-atoms Pt particle can be calculated using the Equation (6) [22]:

$$n = \frac{4\pi r^3}{3V_a} \quad (6)$$

where n is the number of atoms, r the nanoparticle radius and V_a the atomic volume (Pt = 10.20 $cm^3 \cdot mol^{-1}$). In the case of platinum this diameter corresponds to 1.2 nm, therefore there is a tendency to reach this value, considering that the number of amino groups overcome the number of metallic ions per

dendrimer molecule and thus, the size of the particles does not depend of the dendrimer generation but the number of metallic ions [21–23]. Nevertheless, the observed agglomerates suggest the intermolecular complexation of the metal, a typical phenomenon reported for the amino-terminated dendrimers, bearing in mind the high complexation capacity of these groups [20].

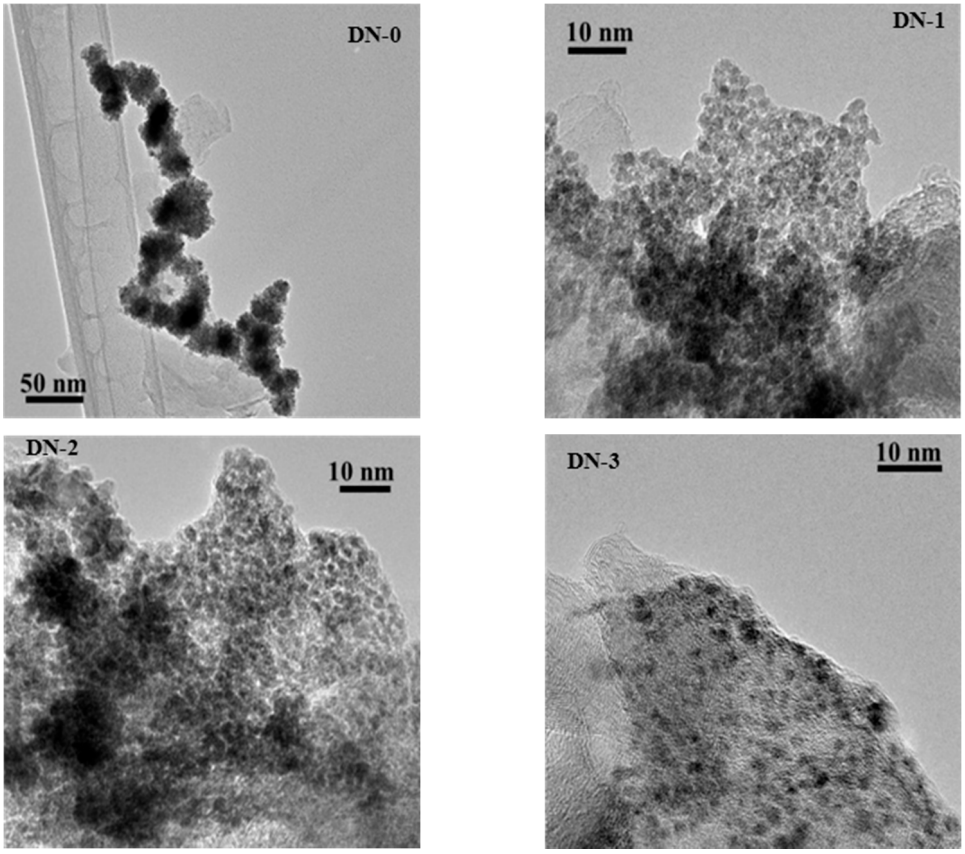

Figure 1. TEM micrographs of the untreated Pt-Ru catalysts synthesized with the 0, 1, 2 and 3 generation dendrimers.

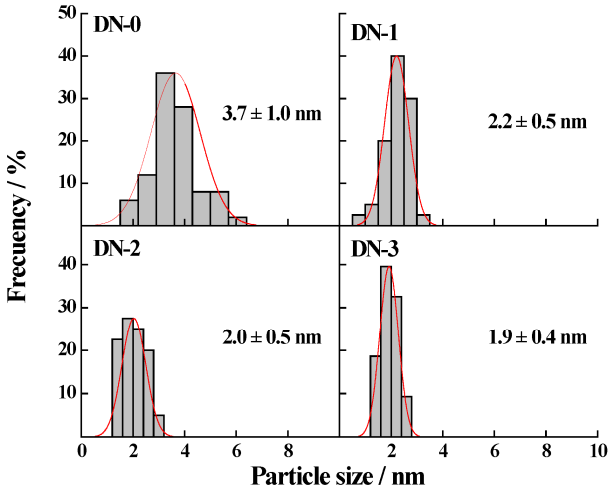

Figure 2. Particle size histograms of the untreated Pt-Ru catalysts synthesized with the 0, 1, 2 and 3 generation dendrimers.

Therefore, it is demonstrated that there is a correlation between the generation of the dendrimer used during the synthesis and the particle dispersion and size: better dispersion and smaller particle size are obtained by increasing the dendrimer generation, that is, the number of branches.

Figure 3 shows the TEM images for the catalysts subjected to the heat treatment at 350 °C, whereas the corresponding particle size distribution is reported in Figure 4. As deduced from Figures 3 and 4, the heat treatment favors the sintering of the nanoparticles. Nevertheless, the sintering degree is less significant for the heat treated materials obtained with higher dendrimer generation. According with this effect, particle size for the catalyst DN-0 increase from 3.7 ± 1.0 to 4.1 ± 1.4 nm after the heat treatment; for DN-2 from 2.0 ± 0.5 to 5.5 ± 1.5 nm; in the case of the material DN-3, the increase is from 1.9 ± 0.4 to 3.1 ± 0.9 nm.

The behavior of the Pt-Ru/CNF-DN-1 TT catalyst was slightly different compared with the other materials. In this case, the particle size did not increase significantly after the heat treatment but the formation of nanorods was observed in some areas of the sample. This fact could be attributed to the presence of dendrimer residues that probably promoted the sintering of some nanoparticles in a fractal direction during the heat treatment, as shown in Figure 5. This behavior as a consequence of the gel de-stabilization process has been already reported by Bigall et al. [65], during the synthesis of Pt aerogels and xerogels.

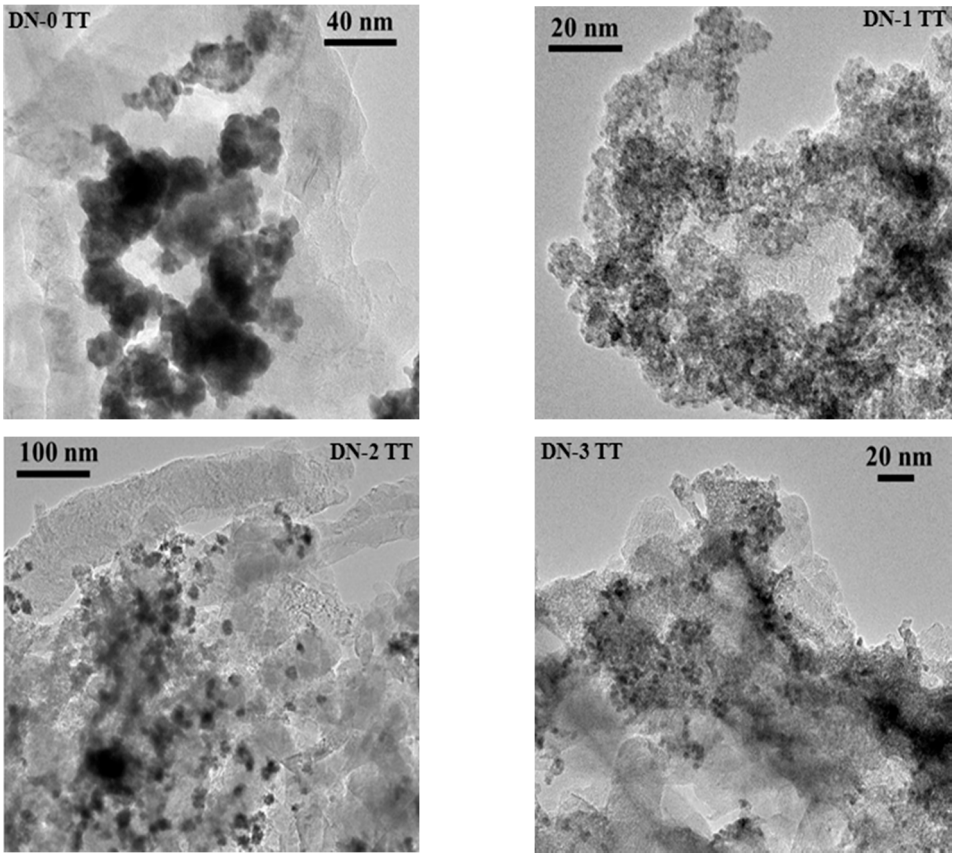

Figure 3. TEM micrographs of the heat treated Pt-Ru catalysts synthesized with the 0, 1, 2 and 3 generation dendrimers.

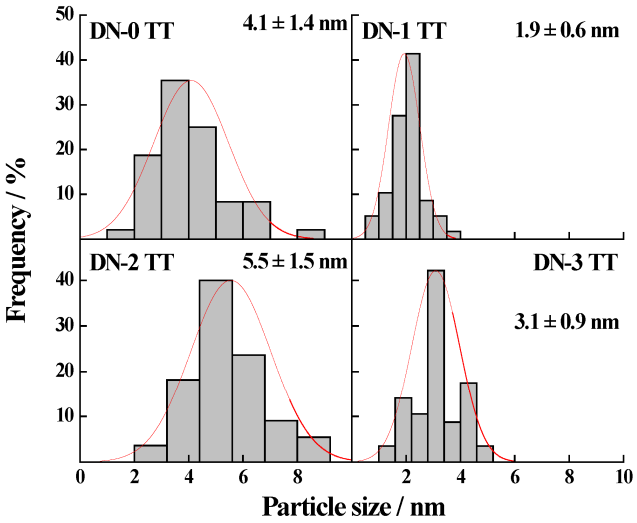

Figure 4. Particle size histograms of the heat treated Pt-Ru catalysts synthesized with the 0, 1, 2 and 3 generation dendrimers.

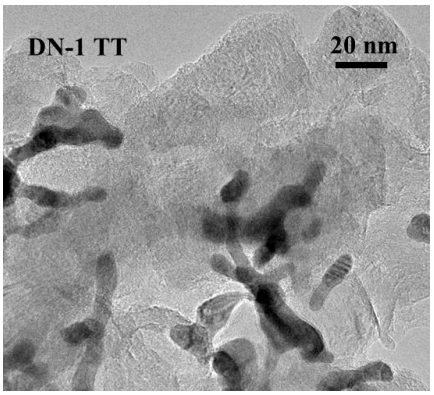

Figure 5. TEM micrographs of Pt-Ru/CNF-DN-1 TT catalyst.

2.2. Activity of Catalysts in the Supporting Electrolyte

Table 1 presents the electrochemical surface areas (ECSA) for the synthesized catalysts, determined from CO stripping measurements reported in [45] (see Figures 4 and 5 in this reference). It was remarkable the decrease of the ECSA for the heat treated materials synthesized with the DN-0 and DN-1 dendrimers, due to the sintering of the nanoparticles. However, in the case of the catalysts prepared with DN-2 and DN-3, this value increased after the heat treatment, as a consequence of the removal of the dendrimer residues favored at 350 °C that increased the number of active sites able to adsorb CO.

Figure 6 presents the electrochemical behavior of the synthesized catalysts in the supporting electrolyte. In the case of the non-heat treated catalysts, the typical signals corresponding to the hydrogen adsorption-desorption process were observed in the range of 0.050–0.2 V vs. RHE. Moreover, high capacitive currents were observed for the catalysts prepared with the DN-0, DN-2 and DN-3 dendrimers, indicating the presence of these molecules adsorbed on the Pt-Ru nanoparticles. These results confirm the ones described above about the agglomeration inhibition due to their encapsulation in the dendrimer structure. The effect of the adsorbed molecules was not evident in the case of the Pt-Ru/CNF-DN-1 catalyst, which exhibited low capacitive current densities.

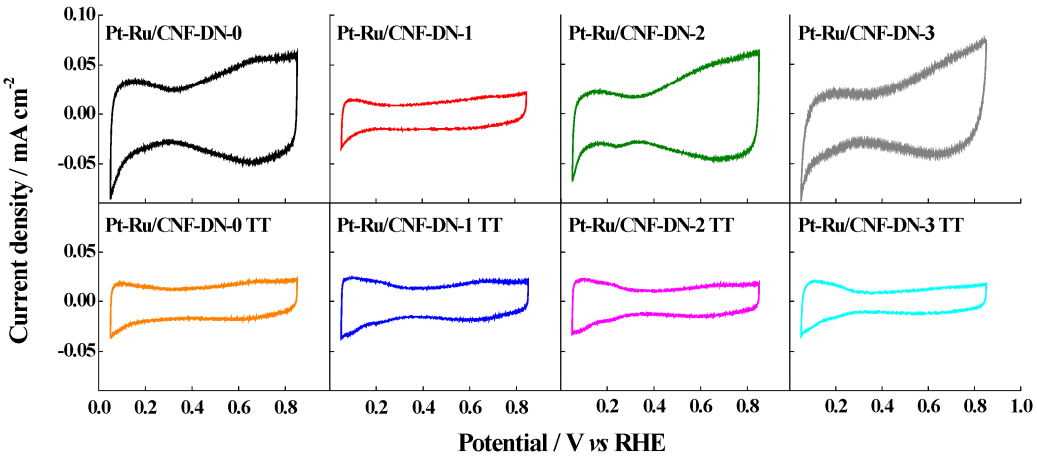

Figure 6. CVs in 0.5 M H_2SO_4 (supporting electrolyte) recorded at 20 $mV \cdot s^{-1}$.

After the heat treatment, the capacitive currents decreased for all the studied catalysts. In fact, the signal for the hydrogen adsorption, located at 0.2 V, is more evident than that of the non-heat treated materials. This result means that the heat treatment efficiently removed the dendrimer residues adsorbed on the catalysts, which remained on them after the synthesis process. The better definition of the electrochemical signals in the supporting electrolyte agrees with those found for the electrochemical oxidation of CO reported in our previous work, which showed an unclear definition of the CO oxidation peak, attributed to the presence of dendrimers covering the surface of the untreated catalysts, and diminished the reactivity towards this adsorbate. The heat treatment removed the organic residues from the catalysts surface, allowing a better definition of these peaks, as shown in Figures 4 and 5 of this work [45].

2.3. Catalytic Activity towards the Methanol Electrochemical Oxidation

In [45], a preliminary electrochemical study at room temperature was performed, in order to assess their catalytic activity. At this temperature, a CO monolayer was adsorbed to appreciate the potential required to oxidize this monolayer and, on the other hand, methanol was also oxidized at room temperature without any mechanistic study, just to identify the current densities generated during this reaction. In the present work, cyclic voltammetry and chronoamperometry studies for the methanol oxidation were performed at six temperatures, in order to obtain novel information about the reaction mechanism and the kinetics of this reaction. Voltamperometric studies of the methanol electrochemical oxidation on the synthesized catalysts were made and the results are presented in Figure 7. The upper panels show a comparison of the electrochemical experiments performed at 20 °C between the heat treated and the untreated materials. In the case of the catalyst prepared with the zero generation dendrimer, the non-heat treated material displayed higher current densities than those observed for the heat treated material, possibly due to a high content of Ru oxides in this material, in agreement with the diffraction peaks observed at 28.5° in the XRD pattern (see Figure 1 in [45]). The presence of Ru oxides was also observed in Pt-Ru/CNF-DN-1 and Pt-Ru/CNF-DN-2 but in a lower extent (see Figure 1 in [45]) and therefore, a smaller effect is expected for these materials. The improved oxidation of the CO_{ad} in the presence of these oxides has been previously reported [29], so these surface oxides could be the responsible of the increase of the methanol oxidation current densities since CO_{ad} is formed as intermediate [30]. Following the same trend, the results observed for the DN-1, DN-2 and DN-3 catalysts are opposite to those found for the DN-0 sample, that is, the heat treated samples displayed higher current densities than the non-heat treated ones as expected from the improvement of active sites due to the removal of the organic species adsorbed on the surface.

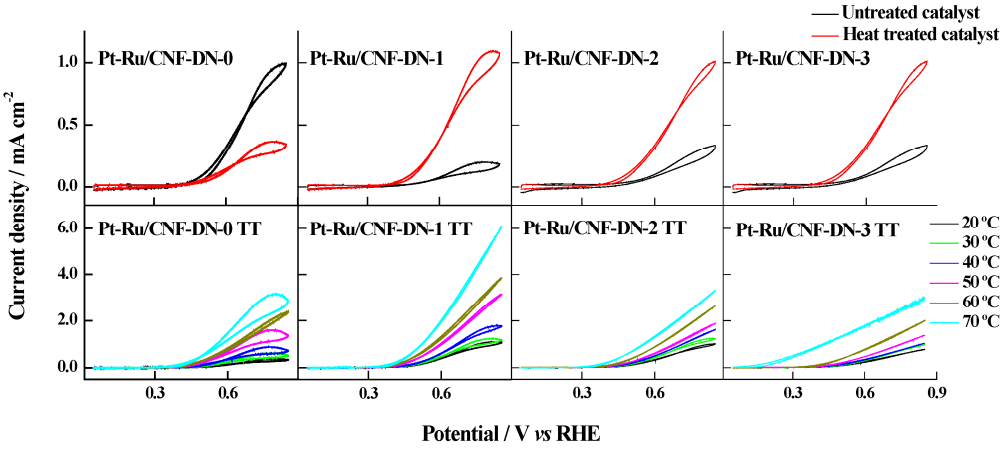

Figure 7. CVs for the methanol oxidation on synthesized catalysts. Upper panel shows the results at 20 °C, whereas lower panel displays the response at different temperatures for the heat treated catalysts. Scan rate: 20 $mV \cdot s^{-1}$. Supporting electrolyte: 0.5 M H_2SO_4. Methanol concentration: 2.0 M.

Particle sizes could play an important role in the activity, bearing in mind that very low diameters have a negative effect in the activity of metallic nanoparticles towards the electrochemical oxidation of methanol. The increase of particle size of at least 10% for materials prepared with DN-2 and DN-3 dendrimers after the heat treatment should explain the increase in activity, but not in the case of the DN-1, as no difference (even a slight decrease) was observed in particle size. So, other effects have to be involved.

The presence of organic residues from the dendrimers was evident from the CO stripping experiments previously published [45] and can contribute to the low registered activities for the catalysts without the heat treatment. The heat treated materials developed the following sequence for the current densities (see Table 2): Pt-Ru/CNF-DN-0 TT < Pt-Ru/CNF-DN-3 TT < Pt-Ru/CNF-DN-2 TT < Pt-Ru/CNF-DN-1 TT

Table 2. Maximum methanol oxidation current densities for the different synthesized catalysts at different temperatures.

Catalyst	Maximum Current Densities/mA·cm^{-2}					
	20 °C	30 °C	40 °C	50 °C	60 °C	70 °C
Pt-Ru/CNF-DN-0 TT	0.39	0.65	0.90	1.63	2.41	3.19
Pt-Ru/CNF-DN-1 TT	1.15	1.25	1.83	3.19	3.92	6.16
Pt-Ru/CNF-DN-2 TT	1.04	1.29	1.64	1.92	2.67	3.35
Pt-Ru/CNF-DN-3 TT	0.81	1.01	1.09	1.39	2.02	2.03
Pt-Ru/C E-TEK	0.29	0.43	0.40	0.48	1.08	1.73

The increase of the current densities for the TT catalysts could also be explained considering the presence of crystalline Ru oxides. A considerable amount of crystalline Ru oxides was established for the Pt-Ru/CNF-DN-3 TT catalyst in [45], although this material is not the one developing the highest current densities for the methanol oxidation. The best catalyst for this reaction is the Pt-Ru/CNF-DN-1 TT. It has to be considered that this is the catalyst exhibiting a characteristic morphology (see Figure 5), with a one direction particle-growth, possibly affecting the performance of this material.

The bottom panels in Figure 7 present the voltamperometric results obtained for the methanol oxidation between 20 and 70 °C on the TT catalysts. The Pt-Ru/CNF-DN-1 TT catalyst developed the highest current densities in the whole temperature range, also displaying low methanol oxidation onset potentials (close to 0.37 V vs. RHE). Particularly, the Pt-Ru/CNF-DN-3 TT catalyst presented an onset potential around 0.15 V at 70 °C. Table 2 shows the maximum methanol oxidation current

densities at the different temperatures (commercial Pt-Ru/E-TEK current values are included for comparison). All the synthesized materials exhibited higher current densities than those observed for the commercial catalyst, in particular the Pt-Ru/CNF-DN-1 TT and Pt-Ru/CNF-DN-2 TT materials. Between 30 and 70 °C, the maximum current densities for the Pt-Ru/CNF-DN-1 TT catalyst were three times higher than those for the commercial one, whereas Pt-Ru/CNF-DN-2 TT and Pt-Ru/CNF-DN-3 TT showed a similar behavior, although the current densities were not so high.

Chronoamperometric curves for the methanol oxidation at the different temperatures were obtained applying potentials closed to typical operation values in a direct methanol fuel cell. Stationary current densities obtained at 0.45 V vs. RHE are given in Figure 8. A current enhancement with the increase of temperature was evident, being the Pt-Ru/CNF-DN-1 TT the one that displayed the most significant effect. The registered values for the stationary current densities at 0.45 V can be seen in Table 3, showing good activities for the catalysts synthesized with the 1, 2 and 3 generation dendrimers, in comparison with the commercial one. In contrast, the catalyst DN-0 TT only overcomes the performance displayed by the E-TEK catalyst at 70 °C.

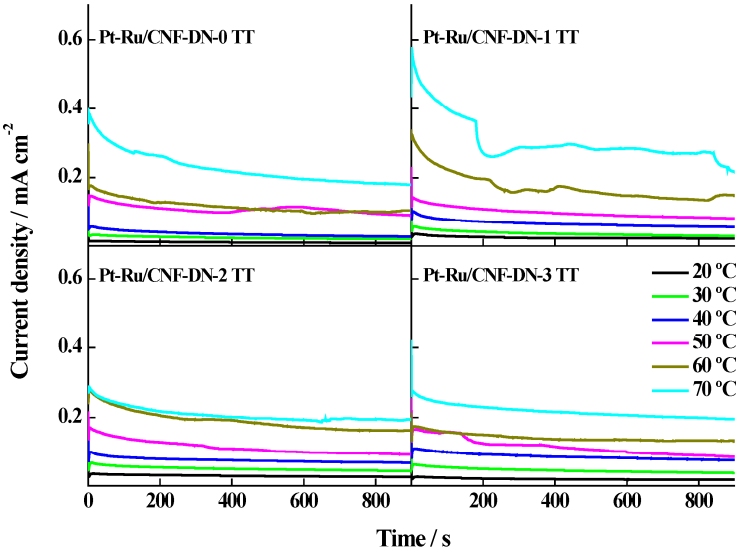

Figure 8. *i–t* curves for methanol oxidation on the synthesized Pt-Ru catalysts. Scan rate: 20 $mV \cdot s^{-1}$. Supporting electrolyte: 0.5 M H_2SO_4. Methanol concentration: 2.0 M. Applied potential: 0.45 V vs. RHE.

Table 3. Stationary methanol oxidation current densities at 0.45 V vs. RHE and apparent activation energies for the different synthesized catalysts.

Catalyst	Stationary Current Densities/mA·cm^{-2}						E_{ap}/kJ·mol^{-1}
	20 °C	30 °C	40 °C	50 °C	60 °C	70 °C	
Pt-Ru/CNF-DN-0 TT	0.01	0.02	0.03	0.10	0.10	0.18	49.8
Pt-Ru/CNF-DN-1 TT	0.02	0.03	0.06	0.09	0.14	0.27	40.2
Pt-Ru/CNF-DN-2 TT	0.03	0.05	0.07	0.10	0.16	0.20	33.4
Pt-Ru/CNF-DN-3 TT	0.02	0.04	0.08	0.09	0.13	0.20	37.4
Pt-Ru/C E-TEK	0.02	——	0.07	——	0.13	0.17	38.6

The chronoamperometric tests were repeated at 0.55 V vs. RHE and the results are shown in Figure 9, whereas the stationary current densities are reported in Table 4. The trends were similar to those observed at 0.45 V: the highest current densities were obtained with Pt-Ru/CNFDN-1 TT. The main difference, respect to the data obtained at 0.45 V, concerns with the increase of the performance

in the case of the catalysts synthesized with the zero generation dendrimer, which displayed higher current densities than Pt-Ru/C E-TEK catalyst.

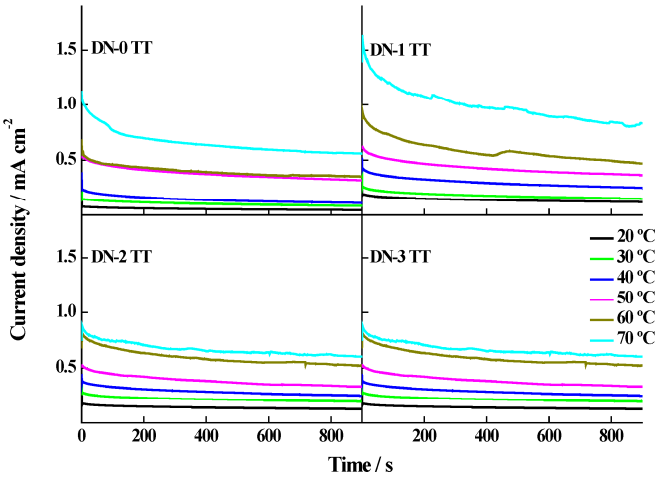

Figure 9. *i–t* curves for the methanol oxidation on the synthesized Pt-Ru catalysts. Scan rate: 20 mV·s^{-1}. Supporting electrolyte: 0.5 M H_2SO_4. Methanol concentration: 2.0 M. Applied potential: 0.55 V vs. RHE.

Table 4. Stationary methanol oxidation current densities at 0.55 V vs. RHE and apparent activation energies for the different synthesized catalysts.

Catalyst	Stationary Current Densities/mA·cm^{-2}						E_{ap}/kJ·mol^{-1}
	20 °C	30 °C	40 °C	50 °C	60 °C	70 °C	
Pt-Ru/CNF-DN-0 TT	0.05	0.09	0.11	0.33	0.36	0.56	42.6
Pt-Ru/CNF-DN-1 TT	0.13	0.16	0.26	0.37	0.50	0.85	32.1
Pt-Ru/CNF-DN-2 TT	0.13	0.20	0.26	0.34	0.53	0.62	26.5
Pt-Ru/CNF-DN-3 TT	0.09	0.15	0.23	0.23	0.43	0.55	28.9
Pt-Ru/C E-TEK	0.05	0.08	0.09	0.11	0.22	0.41	31.6

Using the stationary current density values reported in Tables 3 and 4 and the equations described above (Equations (1)–(4)), the apparent activation energy (E_{ap}) was calculated for the methanol oxidation reaction at 0.45 and 0.55 V for these materials. These values were calculated from the slopes of the Arrhenius plots in Figure 10 and are also reported in Tables 3 and 4. This apparent activation energy implicates a mean value for the total methanol oxidation reaction, which is composed by a set of adsorption and deprotonation steps. In addition, other parallel reactions as the formaldehyde and formic acid production, the formation of adsorbed CO and formate, or the surface diffusion of some species, as the CO surface diffusion, should be considered.

All these reactions depend on the temperature and consequently, the E_{ap} is only a qualitative value used for comparison purposes, being one of them, the identification of rate determining step (*rds*). Thus, the following reaction mechanism is considered [30], which initiates with the adsorption of methanol:

$$CH_3OH \rightleftharpoons CH_3OH_{ads} \quad (7)$$

Then, adsorbed methanol oxidizes by deprotonation to adsorbed CO:

$$CH_3OH_{ads} \rightarrow CO_{ads} + 4H^+ + 4e^- \quad (8)$$

On the other hand, water dissociates on the catalyst surface to produce adsorbed oxygenated species (OH_{ads}) and H^+:

$$H_2O \rightarrow OH_{ads} + H^+ + e^- \quad (9)$$

The final steps consist in the formation of carbon dioxide, by means of the reaction between OH_{ads} and CO_{ads} following these reactions:

$$CO_{ads} + OH_{ads} \rightarrow COOH_{ads} \quad (10)$$

$$COOH_{ads} \rightarrow CO_2 + H^+ + e^- \quad (11)$$

For the first potential (0.45 V, Figure 10a), the E_{ap} values are close to 40 kJ·mol^{-1} (see Table 3), in agreement with the value reported by others authors and associated to the deprotonating alcohol reaction as the *rds* (Reaction (8)) [66,67]. The lowest E_{ap} was observed for the Pt-Ru/CNF-DN-2 TT catalyst, whereas the Pt-Ru/CNF-DN-0 TT catalyst presented the highest E_{ap}, as an evidence of the sintering effect after the heat treatment, which does not favor the catalytic activity of this material. At 0.55 V (Figure 10b), all the slopes decrease in a coherent way, considering that at this higher potential, the reaction is promoted, keeping E_{ap} values between 42.6 kJ·mol^{-1} and 28.9 kJ·mol^{-1}. This fact demonstrated that in some catalysts, with the increase of potential, the *rds* is still the methanol deprotonation, keeping values close to 40 kJ·mol^{-1}, as it is the case of the Pt-Ru/CNF-DN-0 TT and DN-1 TT catalysts. For the catalysts prepared with higher dendrimer generation, this reaction is promoted and E_{ap} decreases. Again, it seems that the presence of crystalline Ru oxides is related with the catalytic behavior, taking into account that the catalysts with the major proportion of these compounds generate the lowest E_{ap}. In this sense, The Pt-Ru/CNF-DN-2 TT and DN-3 TT catalysts displayed E_{ap} values below 29 kJ·mol^{-1}, suggesting the CO_{ads} diffusion to the OH_{ads} (Reaction (10)) as the *rds* for the methanol oxidation, according with the analysis reported by different authors [68–70].

From the analysis carried out in this work considering previous results reported by Calderón et al. [29] related to the effect of the heat treatment on the catalytic activity of Pt-Ru catalysts supported on carbon nanofibers and synthesized by different synthesis methods, it could be inferred that the heat treatment induces the formation of crystalline Ru oxides that promote the increase of the stationary current densities for the methanol oxidation reaction. The Pt-Ru/CNF-DN-1 TT catalyst exhibited the better performance and a different morphology, involving the formation of nanoparticle groups in a determined direction, having particle sizes close to 2.0 nm. Another factor inducing its high activity could be the existence of a suitable Ru oxides/Pt atoms ratio that promotes the methanol oxidation.

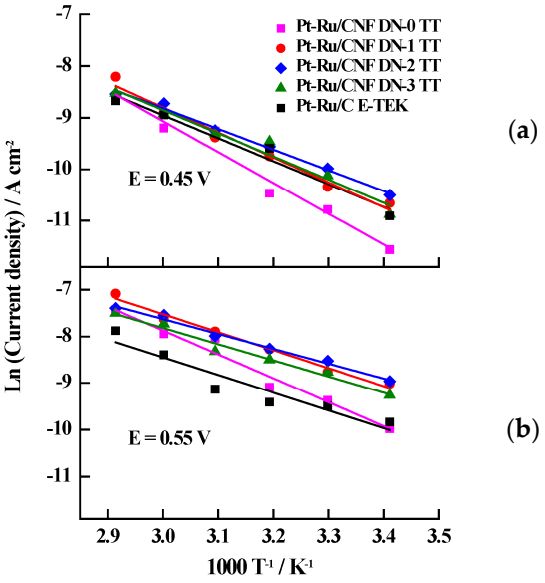

Figure 10. Arrhenius plots for the electrochemical oxidation of methanol at (**a**) 0.45 V and (**b**) 0.55 V on the synthesized catalysts and the commercial Pt-Ru/C E-TEK, at different temperatures.

3. Discussion

The catalytic activity of the synthesized catalysts can be compared with some Pt-Ru catalysts supported on carbon nanofibers or other carbon materials. Actually, we performed a similar kinetic study with Pt-Ru catalysts supported on carbon nanofibers, which were synthesized without any encapsulating agent [71]. In this work, we showed activation energies for the methanol oxidation between 29 and 54 kJ·mol^{-1} at 0.45 V, with the lowest activation energy for the catalyst synthesized by reduction with sodium borohydride. The existence of two slopes for the linear trend in the Arrhenius plots for some catalysts suggests a change in the reaction mechanism from the methanol deprotonation to the CO surface diffusion toward the OH_{ads} around 40–50 °C. This phenomenon was observed in the catalysts reduced with methanol and sodium formate ions. When the applied potential was 0.55 V the activation energies were reduced achieving values among 14 and 45 kJ·mol^{-1} without any change in the slopes. It was conclude that at this potential, the reaction mechanism is addressed basically through the CO surface diffusion toward the OH_{ads}, except in the case of the catalyst reduced with sodium formate ions and heat treated at 350 °C. In the present work, the decrease in the activation energies was related with the dendrimer generation, as a consequence of the enhanced dispersion of the nanoparticles on the carbon supports promoted with the increase of the dendrimer generation, as described previously. Regarding the magnitude of the methanol oxidation stationary current densities, for each of the applied potentials, an increase in the magnitude of these currents was observed in comparison with the catalysts synthesized in [71]. The same behavior was registered for the maximun current densities, which in some cases were close to 6 mA·cm^{-2} in this work, whereas in the case of the materials studied in [71], the maximum values were close to 4 mA·cm^{-2}.

Sebastián et al. [72] supported Pt-Ru nanoparticles on two different carbon nanofibers growth at 600 and 700 °C, which were chemically treated with nitric and a nitric-sulphuric acid mixture, obtaining metal contents and Pt:Ru atomic ratios close to 20 wt. % and 1:1, respectively. The maximum current densities observed for these materials were close to 0.20 mA·cm^{-2} when the carbon nanofibers were synthesized at 600 °C, and 0.25 mA·cm^{-2} for those formed at 700 °C. Particularly, the catalysts supported on nitric acid-treated carbon nanofibers growth at 600 °C, displayed lower current densities than those supported on the nanofibers chemically treated with the nitric-sulphuric acid mixture; however, this trend was inverted when the nanoparticles were supported on the nanofibers formed at 700 °C but chemically treated with the same procedures. It means that the better performance was observed for the catalysts supported on the nitric acid-chemically treated carbon nanofibers growth at 700 °C. This fact was explained from a decrease in the electrochemical surface area with the oxidation of the support. On the other hand, the difference in the performance of these materials, in terms of the temperature employed during the growth of the carbon nanofibers, was attributed to the high graphitized degree achieved at this temperature. The catalysts presented in our work were supported on carbon nanofibers deposited at 700 °C and chemically treated with the nitric-sulphuric acid mixture, which developed higher maximum current densities than those of the catalysts studied in [72].

The performance of Pt-Ru nanoparticles has been also studied when they are supported on other kind of carbon supports such as mesoporous carbons, TiO_2-carbon blacks mixtures and chemically and/or thermally treated carbon blacks [36]. During the tests in the three electrodes-cell, the catalyst supported on carbon black attained the highest methanol oxidation current density at 30 °C (around 0.4 mA·cm^{-2}), which was enhancing until 1.3 mA·cm^{-2} at 60 °C. This behavior was verified in the direct methanol fuel monocell tests, where the catalyst supported on this carbon black displayed the highest current densities (700 mA·cm^{-2}) as well as the best power densities (65 mW·cm^{-2}). The authors determined the activation energy for this reaction, finding values between 42 and 47 kJ·mol^{-1}, suggesting that the methanol deprotonation (see Equation (8)) as the rate determining step route for the reaction. The authors attributed this result to the presence of active carbonyl, hydroxyl or carboxyl surface oxygen groups present on oxidized carbon blacks. The current densities presented in [36] are lower than those in the present manuscript, as well as the apparent activation energies were lower in our study, proving the high activity of the Pt-Ru catalysts synthesized in presence of dendrimers.

Moreover, it must be taken into account that the materials prepared in [36] contain a 30 wt. % as metal content and a Pt:Ru close to 85:15, meaning a higher content of Pt compare with those of our study.

Kinetic parameters of the methanol oxidation have been also determined by varying the scan rate during the methanol oxidation cyclic voltammetries [73]. In the case of Pt-Ru catalysts supported on carbon blacks, Velásquez-Valenzuela et al. found high exchange current densities compared with smooth Pt and Pt/C materials which were explained by the presence of Ru oxides and hydroxides that facilitate the reaction [73]. Changes in the scan rate demonstrated a kinetic reaction control since high values for the Tafel slope were observed, suggesting a slow charge transfer on Pt-Ru/C.

From the comparison between these reports [71–73] and the results in this work, it is possible to conclude that the catalysts prepared in this work have high activity toward the methanol oxidation, in terms of both, high methanol oxidation current densities and low apparent activation energies.

4. Materials and Methods

4.1. Preparation of Carbon Support

Carbon nanofibers were synthesized by catalytic thermal decomposition of methane [74] on a Ni:Cu:Al catalyst. It was prepared by co-precipitation of Ni, Cu and Al nitrates and subsequent calcination at 450 °C, obtaining a final 78:6:16 weight ratio. Before the CNFs growth, it was and activated with a hydrogen flux (20 mL·min^{-1}) at 550 °C for 3 h, in order to reduce the Ni and Cu oxides [75]. CNFs were grown at 700 °C in methane atmosphere for 10 h [75]. Then, they were treated with a HNO_3-H_2SO_4 1:1 (*v*/*v*) mixture during 0.5 h at room temperature, in order to functionalize the surface with oxygen groups [76].

4.2. Pt-Ru/CNF Catalysts Synthesis

Pt-Ru/CNF catalysts with a metal content close to 20 wt. % and Pt:Ru atomic ratio near to 1:1 were synthesized following a previously reported procedure [45]. 2.0 μM PAMAM dendrimer solutions were prepared with each of the different generation molecules (generations 0, 1, 2 and 3 with molecular weights: 516.68, 1429.85, 3256.18 and 6908.84 g·mol^{-1}, respectively; 20 wt. % in methanol, Aldrich (Madrid, Spain) and magnetically stirred for 30 min. Then, an aqueous solution with the desired amount of the metal precursors (H_2PtCl_6, 8 wt. % solution, Aldrich (Madrid, Spain); $RuCl_3$ 99.999 wt. %, Aldrich) was slowly added drop by drop to the dendrimer solution, keeping the agitation during 3 days, in order to assure the total complexing of metal precursors into the molecules. Then, 20 mL of $NaBH_4$ (26.4 mM in 7 M NaOH, Aldrich) were poured dropwise, resulting in a dark color solution indicative of the Pt-Ru nanoparticles formation. After 24 h, carbon nanofibers were added to the reaction mixture under sonication. The reaction mixture was maintained under stirring for 2 days, and finally filtered, washed with ultrapure water and dried at 60 °C during 2 h. The Pt-Ru nanoparticles supported on CNFs prepared by using dendrimers were labelled as Pt-Ru/CNF-DN-X, being X the dendrimer generation employed during the synthesis procedure. Finally, the synthesized catalysts were heat treated at 350 °C in O_2-atmosphere for 30 min, generating materials designated as Pt-Ru/CNF-DN-X TT.

4.3. Physicochemical Characterization

Energy dispersive X-ray (EDX) characterization was employed for determining the metal content and Pt:Ru atomic ratio of the synthesized materials. For these analyzes, an 6699 ATW scanning electron microscope (located at SEGAI-ULL, Tenerife, Spain; Oxford Instruments Microanalysis Group, (Abingdon, UK), working at 20 keV, with a Si detector and a Be window was used. X-ray diffraction (XRD) patterns were obtained by means of an X'Pert, universal diffractometer (Panalytical, Almelo, The Netherlands) operating with Cu-Kα radiation, generated at 40 kV and 30 mA. Scan rate was 3° min^{-1} with 2θ values between 10° and 100°. Scherrer's equation was applied to determine the metal crystallite size from XRD, using the (220) peak around 2θ = 70°, while Vegard's law was utilized for

the calculation of the lattice parameter [45]. A 200 kV JEM 2100 transmission electron microscope (JEOL, Peabody, MA, USA) was used for carrying out the TEM analyses. An aliquot from an ethanol suspension of the catalysts was drop cast on a carbon grid. A MultiScan CCD (Gatan 794, Pleasanton, CA, USA) camera was employed to obtain the images, which were treated with the Fourier Transform software Digital Micrograh (Gatan 3.7.0), measuring more than 200 nanoparticle diameters in order to generate the particle size distribution histograms.

4.4. Electrochemical Characterization

An electrochemical thermostatized cell was used with a glassy carbon disk as working electrode, while the counter electrode was a glassy carbon bar and a reversible hydrogen electrode (RHE), placed inside a Luggin capillary, worked as reference electrode. The potentials in the present article are referred to the RHE electrode. To prepare the catalyst layer on the working electrode, a homogeneous suspension was prepared by mixing 2 mg of catalyst, 15 μL of Nafion (5 wt. %, Aldrich), and 500 μL of ultrapure water. A 60 μL-aliquot was deposited onto the glassy carbon disk. 0.5 M H_2SO_4 (95%–97%, Merck, Madrid, Spain) solution was used in these experiments as supporting electrolyte. Electrochemical surface areas (ECSA) were estimated from the CO stripping experiments, assuming a charge of 420 $\mu C \cdot cm^{-2}$ [77]. All the currents presented in this work have been normalized with these electrochemical surface areas. Previous works reported the CO reactivity on the different catalysts [45,46] between 20 and 70 °C. This experiment consisted of bubbling of CO into the electrochemical cell for 10 min, producing an adsorbed CO monolayer on the deposited catalyst. Then, nitrogen (MicroGeN_2, GasLab, Fremont, CA, USA) was bubbled during 10 min to remove CO from the solution. For methanol (98%, Merck) experiments, 2.0 M solution in the supporting electrolyte was used, performing potential scans between 0.050 and 0.85 V at 20 $mV \cdot s^{-1}$. Current transient curves in presence of methanol were obtained by applying potential steps from 0.05 V to typical direct methanol fuel cell operation potential values for the anode such as 0.45 and 0.55 V. The experiments were made in a temperature range of 20–70 °C. The electrochemical measurements were recorded using a μAUTOLAB III modular equipment system (Metrohm, Herisau, Switzerland).

5. Conclusions

Pt-Ru catalysts supported on carbon nanofibers were prepared using dendrimers of zero, one, two and three generation, and sodium borohydride as reducing agent. All catalysts exhibited metal loadings and Pt:Ru atomic ratios close to 20 wt. % and 1:1, respectively. The use of dendrimers during the synthesis did not assure a good distribution of the nanoparticles on the carbon support. The 1-generation dendrimer induced the sintering of the nanoparticles in one direction, in the case of the catalyst Pt-Ru/CNF-DN-1-TT, modifying the morphology patterns observed for the other materials.

The increase of the dendrimer generation induced a decrease in both the particle average size and aggregation on the carbon support. Heat treatment of the catalysts resulted in an increase of the particle size as well as the formation of crystalline Ru oxides. As a consequence of the oxides formation, an increase in the catalytic activity was observed in terms of higher current densities for methanol oxidation. The best results were obtained for Pt-Ru/CNF-DN-1 TT, the material with the special morphology induced by the heat treatment.

Activation energies for methanol oxidation reactions were determined, allowing the achievement of some conclusions on the rate determining step. In this sense, it was observed that at 0.45 V the *rds* was the deprotonation of methanol for all the catalysts, whereas at 0.55 V, the *rds* was the CO_{ad} diffusion for the Pt-Ru/CNF-DN-2 TT and Pt-Ru/CNF-DN-3 TT catalysts. These results allow to conclude that both the dendrimer generation and the heat treatment determine the morphological properties of the catalysts, conditioning the final electrochemical properties.

Acknowledgments: This work was carried out with the support of Ministry of Economy and Competitiveness (MINECO) through the project ENE2014-52158-C2-2-R and 1-R (co-funded by FEDER). J.C.C. is indebted to the Alβan Program for the predoctoral fellowship No. E07D403742CO. Authors want to thank the Institute of

Catalysis and Petrochemistry (CSIC) for the TEM analysis, as well as the General Support Services for Research of Universidad de La Laguna (SEGAI) for the EDX and XRD analysis of the synthesized catalysts.

Author Contributions: J.C.C. synthesized the catalysts and performed the experiments, wrote the paper. L.C. synthesized the carbon nanofibers. M.J.L. and E.P. contributed reagents/materials/analysis tools. J.C.C., J.L.R. and E.P. conceived and designed the experiments. L.C., J.L.R., M.J.L. and E.P. revised the manuscript.

Conflicts of Interest: The authors declare no conflict of interest.

References

1. Tomalia, D.A.; Naylor, A.; Goddard, W.A. Starburst Dendrimers: Molecular-Level Control of Size, Shape, Surface Chemistry, Topology, and Flexibility from Atoms to Macroscopic Matter. *Angew. Chem. Int. Ed. Engl.* **1967**, *29*, 138–175. [CrossRef]
2. Fréchet, J.M.J. Functional Polymers and Dendrimers: Reactivity, Molecular Architecture and Interfacial Energy. *Science* **1994**, *263*, 1710–1715. [CrossRef] [PubMed]
3. Ardoin, N.; Astruc, D. The Molecular Trees: From Syntheses towards Applications. *Bull. Soc. Chim. Fr.* **1995**, *132*, 875–909.
4. Bosman, A.W.; Janssen, H.M.; Meijer, E.W. About Dendrimers: Structure, Physical Properties and Applications. *Chem. Rev.* **1999**, *99*, 1665–1688. [CrossRef] [PubMed]
5. Zhao, M.; Sun, L.; Crooks, R.M. Preparation of Cu Nanoclusters within Dendrimer Templates. *J. Am. Chem. Soc.* **1998**, *120*, 4877–4878. [CrossRef]
6. Zhao, M.; Crooks, R.M. Homogeneous Hydrogenation Catalysis with Monodisperse, Dendrimer-Encapsulated Pd and Pt Nanoparticles. *Angew. Chem. Int. Ed.* **1999**, *38*, 364–366. [CrossRef]
7. Chechik, V.; Zhao, M.; Crooks, R.M. Self-Assembled Inverted Micelles Prepared from a Dendrimer Template: Phase Transfer of Encapsulated Guests. *J. Am. Chem. Soc.* **1999**, *121*, 4910–4911. [CrossRef]
8. Tokuhisa, H.; Zhao, M.; Baker, L.A. Preparation and Characterization of Dendrimer Monolayers and Dendrimer-Alkanethiolmixed Monolayers Adsorbed to Gold. *J. Am. Chem. Soc.* **1998**, *120*, 4492–4501. [CrossRef]
9. Jansen, J.F.G.A.; de Brabander-van den Berg, E.M.M.; Meijer, E.W. Encapsulation of Guest Molecules into a Dendritic Box. *Science* **1994**, *266*, 1226–1229. [CrossRef] [PubMed]
10. Crooks, R.M.; Zhao, M.; Sun, L.; Chechik, V.; Yeung, L.K. Dendrimer-Encapsulated Metal Nanoparticles: Synthesis, Characterization and Applications to Catalysis. *Acc. Chem. Res.* **2001**, *34*, 181–190. [CrossRef] [PubMed]
11. Lang, H.; May, R.A.; Iversen, B.L.; Chandler, B.D. Dendrimer-Encapsulated Nanoparticle Precursors to Supported Platinum Catalysts. *J. Am. Chem. Soc.* **2003**, *125*, 14832–14836. [CrossRef] [PubMed]
12. Kreibig, U.; Vollmer, M. *Optical Properties of Metal Clusters*, 1st ed.; Springer: Berlín, Germany, 1995; pp. 203–274.
13. Curtis, A.C.; Duff, D.G.; Edwards, P.P.; Jefferson, D.A.; Johnson, B.F.G.; Kirkland, A.I.; Wallace, A.S. A Morphology-Selective Copper Organosol. *Angew. Chem. Int. Ed.* **1988**, *27*, 1530–1533. [CrossRef]
14. Lisiecki, I.; Pileni, M.P. Synthesis of Copper Metallic Clusters Using Reverse Micelles as Microreactors. *J. Am. Chem. Soc.* **1993**, *115*, 3887–3896. [CrossRef]
15. Singh, A.; Chandler, B.D. Low-Temperature Activation Conditions for PAMAM Dendrimer Templated Pt Nanoparticles. *Langmuir* **2005**, *21*, 10776–10782. [CrossRef] [PubMed]
16. Beakley, L.W.; Yost, S.E.; Cheng, R.; Chandler, B.D. Nanocomposite Catalysts: Dendrimer Encapsulated Nanoparticles Immobilized in Sol-Gel Silica. *Appl. Catal.* **2005**, *292*, 124–129. [CrossRef]
17. Wu, H.; Liu, Z.; Wang, X.; Zhao, B.; Zhang, J.; Li, C. Preparation of Hollow Capsule-Stabilized Gold Nanoparticles through the Encapsulation of the Dendrimer. *J. Colloid Interface Sci.* **2006**, *302*, 142–148. [CrossRef] [PubMed]
18. Crespilho, F.N.; Huguenin, F.; Zucolotto, V.; Olivi, P.; Nart, F.C.; Oliveira, O.N., Jr. Dendrimers as Nanoreactors to Produce Platinum Nanoparticles Embedded in Layer by Layer Films for Methanol-Tolerant Cathodes. *Electrochem. Commun.* **2006**, *8*, 348–352. [CrossRef]
19. Scott, R.W.J.; Datye, A.K.; Crooks, R.M. Bimetallic Palladium-Platinum Dendrimer Encapsulated Catalysts. *J. Am. Chem. Soc.* **2003**, *125*, 3708–3709. [CrossRef] [PubMed]

20. Chung, Y.M.; Rhee, H.K. Synthesis and Catalytic Applications of Dendrimer-Templated Bimetallic Nanoparticles. *Catal. Surv. Asia* **2004**, *8*, 211–223. [CrossRef]
21. Niu, Y.; Yeung, L.K.; Crooks, R.M. Size-Selective Hydrogenation of Olefins by Dendrimer-Encapsulated Palladium Nanoparticles. *J. Am. Chem. Soc.* **2001**, *123*, 6840–6846. [CrossRef]
22. García-Martinez, J.C.; Crooks, R.M. Extraction of Au Nanoparticles Having Narrow Size Distributions from within Dendrimer Templates. *J. Am. Chem. Soc.* **2004**, *126*, 16170–16178. [CrossRef] [PubMed]
23. Lemo, J.; Heuzé, K.; Astruc, D. Synthesis and Catalytic Activity of DAB-Dendrimer Encapsulated Pd Nanoparticles for the Suzuki Coupling Reaction. *Inorg. Chim. Acta* **2006**, *359*, 4909–4911. [CrossRef]
24. Peng, X.; Pan, Q.; Rempel, G.L.; Wu, S. Synthesis, Characterization and Application of PdPt and PdRh Bimetallic Nanoparticles Encapsulated within Amine-Terminated Poly(amidoamine) Dendrimers. *Catal. Commun.* **2009**, *11*, 62–66. [CrossRef]
25. Crooks, R.M.; Zhao, M. Dendrimer-Encapsulated Pt Nanoparticles: Synthesis, Characterization and Applications to Catalysis. *Adv. Mater.* **1999**, *11*, 217–220. [CrossRef]
26. Zhang, W.; Li, L.; Du, Y.; Wang, X.; Yang, P. Gold/Platinum Bimetallic Core/Shell Nanoparticles Stabilized by a Frechet Type Dendrimer: Preparation and Catalytic Hydrogenations of Phenylaldehydes and Nitrobenzenes. *Catal. Lett.* **2009**, *127*, 429–436. [CrossRef]
27. Niu, Y.; Sun, L.; Crooks, R.M. Determination of the Intrinsic Proton Binding Constants for Poly(amidoamine) Dendrimers via Potentiometric pH Titration. *Macromolecules* **2003**, *36*, 5725–5731. [CrossRef]
28. Ye, H.; Scott, R.W.J.; Crooks, R.M. Synthesis, Characterization and Surface Immobilization of Platinum and Palladium Nanoparticles Encapsulated within Amine-Terminated Poly(amidoamine) Dendrimers. *Langmuir* **1999**, *20*, 2915–2920. [CrossRef]
29. Calderón, J.C.; García, G.; Calvillo, L.; Rodríguez, J.L.; Lázaro, M.J.; Pastor, E. Electrochemical Oxidation of CO and Methanol on Pt-Ru Catalysts Supported on Carbon Nanofibers: The Influence of Synthesis Method. *Appl. Catal. B Environ.* **2015**, *165*, 676–686.
30. Watanabe, M.; Motoo, S. Electrocatalysis by Ad-Atoms: Part II. Enhancement of the Oxidation of Methanol on Platinum by Ruthenium Ad-Atoms. *J. Electroanal. Chem.* **1975**, *60*, 267–273. [CrossRef]
31. Gasteiger, H.A.; Markovic, N.M.; Ross, P.N., Jr. H_2 and CO Electrooxidation on Well Characterized Pt, Ru, and Pt-Ru. 1. Rotating Disk Electrode Studies of the Pure Gases Including Temperature Effects. *J. Phys. Chem.* **1995**, *99*, 8290–8301. [CrossRef]
32. Harada, M.; Einaga, H. Preparation of Pt/Rh Bimetallic Colloidal Particles in Polymer Solutions Using Borohydride-Reduction. *J. Colloid Interface Sci.* **2007**, *308*, 568–572. [CrossRef] [PubMed]
33. Nagao, D.; Shimazaki, Y.; Saeki, S.; Kobayashi, Y.; Konno, M. Effect of Ultrasonic Irradiation on Carbon-Supported Pt-Ru Nanoparticles Prepared at High Metal Concentrations. *Colloid Surf.* **2007**, *302*, 623–627. [CrossRef]
34. Gonzalez, E.R.; Ticianelli, E.A.; Pinheiro, A.L.N.; Perez, J. Processo de obtenção de catalisador de platina dispersa ancorada em substrato através da redução por ácido. Brazilian Patent INPI-SP No. 00321, 2 September 1997.
35. Lizcano-Valbuena, W.H.; Paganin, V.A.; González, E.R. Methanol Electro-Oxidation on Gas Diffusion Electrodes Prepared with Pt-Ru/C Catalysts. *Electrochim. Acta* **2002**, *47*, 3715–3722. [CrossRef]
36. Salgado, J.R.C.; Paganin, V.A.; González, E.R.; Montemor, M.F.; Tacchini, I.; Ansón, A.; Salvador, M.A.; Ferreira, P.; Figueiredo, F.M.L.; Ferreira, M.G.S. Characterization and Performance Evaluation of Pt-Ru Electrocatalysts Supported on Different Carbon Materials for Direct Methanol Fuel Cells. *Int. J. Hydrog. Energy* **2013**, *38*, 910–920. [CrossRef]
37. Dos Santos, L.; Colmati, F.; González, E.R. Preparation and Characterization of Supported Pt-Ru Catalysts with a High Ru Content. *J. Power Sources* **2006**, *159*, 869–877. [CrossRef]
38. Wang, X.; Hsing, I.M. Surfactant Stabilized Pt and Pt Alloy Electrocatalyst for Polymer Electrolyte Fuel Cells. *Electrochim. Acta* **2002**, *47*, 2981–2987. [CrossRef]
39. Yan, S.; Sun, G.; Tian, J.; Jiang, L.; Qi, J.; Xin, Q. Polyol Synthesis of Highly Active PtRu/C Catalyst with High Metal Loading. *Electrochim. Acta* **2006**, *52*, 1692–1696. [CrossRef]
40. Liu, Z.; Hong, L. Electrochemical Characterization of the Electrooxidation of Methanol, Ethanol and Formic Acid on Pt/C and PtRu/C Electrodes. *J. Appl. Electrochem.* **2007**, *37*, 505–510. [CrossRef]

41. Kanninen, P.; Borghei, M.; Ruiz, V.; Kauppinen, E.I.; Kallio, T.; Yi, J. The Effect of Nafion Content in a Graphitized Carbon Nanofiber-Based Anode for the Direct Methanol Fuel Cell. *Int. J. Hydrog. Energy* **2012**, *37*, 19082–19091. [CrossRef]
42. Sebastián, D.; Suelves, I.; Pastor, E.; Moliner, R.; Lázaro, M.J. The Effect of Carbon Nanofiber Properties as Support for Pt-Ru Nanoparticles on the Electrooxidation of Alcohols. *Appl. Catal. B Environ.* **2013**, *132*, 13–21. [CrossRef]
43. Alegre, C.; Gálvez, M.E.; Moliner, R.; Baglio, V.; Stassi, A.; Aricò, A.S.; Lázaro, M.J. Platinum Ruthenium Catalysts Supported on Carbon Xerogel for Methanol Electro-Oxidation: Influence of the Catalyst Synthesis Method. *ChemCatChem* **2013**, *5*, 3770–3780. [CrossRef]
44. Gu, Y.; Wu, G.; Hu, X.F.; Chen, D.A.; Hansen, T.; Zur Loye, H.C.; Ploehn, H.J. PAMAM-Stabilized Pt-Ru Nanoparticles for Methanol Electro-Oxidation. *J. Power Sources* **2010**, *195*, 425–434. [CrossRef]
45. Calderón, J.C.; Calvillo, L.; Lázaro, M.J.; Pastor, E. Use of Dendrimers during the Synthesis of Pt-Ru Electrocatalysts for PEM Fuel Cells: Effects on the Physical and Electrochemical Properties. *Int. J. Electrochem.* **2011**. [CrossRef]
46. Calderón, J.C.; Calvillo, L.; Lázaro, M.J.; Rodríguez, J.L.; Pastor, E. CO Electrochemical Oxidation on Dendrimers-Synthesized Pt-Ru Catalysts Supported on Carbon Nanofibers: A Kinetic Study. *Ciênc. Tecnol. Mater.* **2012**, *24*, 176–179.
47. McBreen, J.; Olender, H.; Srinivasan, S.; Kordesch, K. Carbon Supports for Phosphoric Acid Fuel Cell Electrocatalysts: Alternative Materials and Method of Evaluations. *J. Appl. Electrochem.* **1981**, *11*, 787–796. [CrossRef]
48. Uchida, M.; Aoyama, Y.; Tanabe, M.; Yanagihara, N.; Eda, N.; Ohta, A. Influences of both Carbon Supports and Heat-Treatment of Supported Catalyst on Electrochemical Oxidation of Methanol. *J. Electrochem. Soc.* **1995**, *142*, 2572–2576. [CrossRef]
49. Pantea, D.; Darmstadt, H.; Kaliaguine, S.; Sümmchen, L.; Roy, C. Electrical Conductivity of Thermal Carbon Blacks: Influence of Surface Chemistry. *Carbon* **2001**, *39*, 1147–1158. [CrossRef]
50. Jun, S.; Joo, S.H.; Ryoo, R.; Kruk, M.; Jaroniec, M.; Liu, Z.; Ohsuna, T.; Terasaki, O. Synthesis of New Nanoporous Carbon with Hexagonally Ordered Mesostructure. *J. Am. Chem. Soc.* **2000**, *122*, 10712–10713. [CrossRef]
51. Chang, H.; Joo, S.H.; Pak, C. Synthesis and Characterization of Mesoporous Carbons for Fuel Cells Applications. *J. Mater. Chem.* **2007**, *17*, 3078–3088. [CrossRef]
52. Calvillo, L.; Lázaro, M.J.; Bordejé, E.G.; Moliner, R.; Cabot, P.L.; Esparbé, I.; Pastor, E.; Quintana, J.J. Platinum Supported on Functionalized Ordered Mesoporous Carbon as Electrocatalyst for Direct Methanol Fuel Cells. *J. Power Sources* **2007**, *169*, 59–64. [CrossRef]
53. Alegre, C.; Gálvez, M.E.; Baquedano, E.; Moliner, R.; Pastor, E.; Lázaro, M.J. Oxygen-Functionalized Highly Mesoporous Carbon Xerogel Based Catalysts for Direct Methanol Fuel Cell Anodes. *J. Phys. Chem. C* **2013**, *117*, 13045–13058. [CrossRef]
54. Park, I.S.; Park, K.W.; Choi, J.H.; Park, C.R.; Sung, Y.E. Electrocatalytic Enhancement of Methanol Oxidation by Graphite Nanofibers with a High Loading of PtRu Alloy Nanoparticles. *Carbon* **2007**, *45*, 28–33. [CrossRef]
55. Cohen, J.L.; Volpe, D.J.; Abruña, H.D. Electrochemical Determination of Activation Energies for Methanol Oxidation on Polycrystalline Platinum in Acidic and Alkaline Electrolytes. *Phys. Chem. Chem. Phys.* **2007**, *9*, 49–77. [CrossRef] [PubMed]
56. Drazic, D.M.; Drazic, V. Nature of the Rest Potential of Platinum Electrodes in Alkaline Alcohol Solutions. *Electrochim. Acta* **1966**, *11*, 1235–1241. [CrossRef]
57. Chu, D.; Gilman, S. Methanol Electro-Oxidation on Unsupported Pt-Ru Alloys at Different Temperatures. *J. Electrochem. Soc.* **1996**, *143*, 1685–1690. [CrossRef]
58. Tremiliosi-Filho, G.; Kim, H.; Chrzanowski, W.; Wieckowski, A.; Grzybowska, B.; Kulesza, P. Reactivity and Activation Parameters in Methanol Oxidation on Platinum Single Crystal Electrodes 'Decorated' by Ruthenium Adlayers. *J. Electroanal. Chem.* **1999**, *467*, 143–156. [CrossRef]
59. Madden, T.H.; Stuve, E.M. Mechanisms of Elevated Temperature Methanol Electro-Oxidation and Poisoning on Pt/C-Nafion Catalyst Layers. *J. Electrochem. Soc.* **2003**, *150*, E571–E577. [CrossRef]
60. Gasteiger, H.A.; Ross, P.N., Jr.; Cairns, E.J. LEIS and AES on Sputtered and Annealed Polycrystalline Pt-Ru Bulk Alloys. *Surf. Sci.* **1993**, *293*, 67–80. [CrossRef]

61. Radmilovic, V.; Gasteiger, H.A.; Ross, P.N. Structure and Chemical Composition of a Supported Pt-Ru Electrocatalyst for Methanol Oxidation. *J. Catal.* **1995**, *154*, 98–106. [CrossRef]
62. Suryanarayana, C.; Grant, N.M. *X-ray Diffraction: A Practical Approach*, 1st ed.; Plenum Press: New York, NY, USA, 1998.
63. Jiqiao, L.; Baiyun, H. Particle Size Characterization of Ultrafine Tungsten Powder. *Int. J. Refract. Met. Hard Mater.* **2001**, *19*, 89–99. [CrossRef]
64. Carmo, M.; dos Santos, A.R.; Poco, J.G.R.; Linardi, M. Physical and Electrochemical Evaluation of Commercial Carbon Black as Electrocatalysts Supports for DMFC Applications. *J. Power Sources* **2007**, *173*, 860–866. [CrossRef]
65. Bigall, N.C.; Eychmüller, A. Synthesis of Noble Metal Nanoparticles and their Non-Ordered Superstructures. *Philos. Trans. R. Soc. A* **2010**, *368*, 1385–1404. [CrossRef] [PubMed]
66. Tripkovic, A.V.; Strbac, S.; Popovi, K.D. Effect of Temperature on the Methanol Oxidation at Supported Pt and PtRu Catalysts in Alkaline Solution. *Electrochem. Commun.* **2003**, *5*, 484–490. [CrossRef]
67. Guillén-Villafuerte, O.; García, G.; Guil-López, R.; Nieto, E.; Rodríguez, J.L.; Fierro, J.L.G.; Pastor, E. Carbon Monoxide and Methanol Oxidations on Pt/X@MoO_3/C (X = Mo_2C, MoO_2, Mo^0) Electrodes at Different Temperatures. *J. Power Sources* **2013**, *231*, 163–172. [CrossRef]
68. Poelsema, B.; Verheij, L.K.; Comsa, G. He-Scattering Investigation of CO Migration on Pt (111). *Phys. Rev. Lett.* **1982**, *49*, 1731–1735. [CrossRef]
69. Reutt-Robey, J.E.; Doren, D.J.; Chabal, Y.J.; Christman, S.B. CO Diffusion on Pt (111) with Time-Resolved Infrared-Pulsed Molecular Beam Methods: Critical Tests and Analysis. *J. Chem. Phys.* **1990**, *93*, 9113–9129. [CrossRef]
70. Croci, M.; Félix, C.; Vandoni, G.; Harbich, W.; Monot, R. Measurement of Macroscopic Diffusion of CO on Pt (111) by Thermal Helium Scattering. *Surf. Sci. Lett.* **1993**, *290*, L667–L672.
71. Calderón, J.C.; García, G.; Querejeta, A.; Alcaide, F.; Calvillo, L.; Lázaro, M.J.; Rodríguez, J.L.; Pastor, E. Carbon Monoxide and Methanol Oxidations on Carbon Nanofibers Supported Pt–Ru Electrodes at Different Temperatures. *Electrochim. Acta* **2015**, *186*, 359–368.
72. Sebastián, D.; Lázaro, M.J.; Moliner, R.; Suelves, I.; Aricò, A.S.; Baglio, V. Oxidized Carbon Nanofibers Supporting PtRu Nanoparticles for Direct Methanol Fuel Cells. *Int. J. Hydrog. Energy* **2014**, *39*, 5414–5423. [CrossRef]
73. Velázquez-Palenzuela, A.; Centellas, F.; Garrido, J.A.; Arias, C.; Rodríguez, R.M.; Brillas, E.; Cabot, P.L. Kinetic Analysis of Carbon Monoxide and Methanol Oxidation on High Performance Carbon-Supported Pt-Ru Electrocatalyst for Direct Methanol Fuel Cells. *J. Power Sources* **2011**, *196*, 3503–3512. [CrossRef]
74. Suelves, I.; Lázaro, M.J.; Moliner, R.; Corbella, B.M.; Palacios, J.M. Hydrogen Production by Thermo Catalytic Decomposition of Methane on Ni-Based Catalysts: Influence of Operating Conditions on Catalyst Deactivation and Carbon Characteristics. *Int. J. Hydrog. Energy* **2005**, *30*, 1555–1567. [CrossRef]
75. Suelves, I.; Lázaro, M.J.; Moliner, R.; Echegoyen, Y.; Palacios, J.M. Characterization of NiAl and NiCuAl Catalysts Prepared by Different Methods for Hydrogen Production by Thermo Catalytic Decomposition of Methane. *Catal. Today* **2006**, *116*, 271–280. [CrossRef]
76. Calvillo, L.; Lázaro, M.J.; Suelves, I.; Echegoyen, Y.; Bordejé, E.G.; Moliner, R. Study of the Surface Chemistry of Modified Carbon Nanofibers by Oxidation Treatments in Liquid Phase. *J. Nanosci. Nanotechnol.* **2009**, *9*, 4164–4169. [CrossRef] [PubMed]
77. Trassatti, S.; Petrii, O.A. Real Surface Area Measurements in Electrochemistry. *Pure Appl. Chem.* **1991**, *63*, 711–734. [CrossRef]